

## Early age hydration of model slag cement

### Interaction among $C_3S$ , gypsum and slag with different $Al_2O_3$ contents

Zhang, Yu; Wan, Zhi; de Lima Junior, Luiz Miranda; Çopuroğlu, Oğuzhan

**DOI**

[10.1016/j.cemconres.2022.106954](https://doi.org/10.1016/j.cemconres.2022.106954)

**Publication date**

2022

**Document Version**

Final published version

**Published in**

Cement and Concrete Research

**Citation (APA)**

Zhang, Y., Wan, Z., de Lima Junior, L. M., & Çopuroğlu, O. (2022). Early age hydration of model slag cement: Interaction among  $C_3S$ , gypsum and slag with different  $Al_2O_3$  contents. *Cement and Concrete Research*, 161, Article 106954. <https://doi.org/10.1016/j.cemconres.2022.106954>

**Important note**

To cite this publication, please use the final published version (if applicable). Please check the document version above.

**Copyright**

Other than for strictly personal use, it is not permitted to download, forward or distribute the text or part of it, without the consent of the author(s) and/or copyright holder(s), unless the work is under an open content license such as Creative Commons.

**Takedown policy**

Please contact us and provide details if you believe this document breaches copyrights. We will remove access to the work immediately and investigate your claim.



# Early age hydration of model slag cement: Interaction among $C_3S$ , gypsum and slag with different $Al_2O_3$ contents

Yu Zhang<sup>\*</sup>, Zhi Wan, Luiz Miranda de Lima Junior, Oğuzhan Çopuroğlu

Microlab, Faculty of Civil Engineering and Geosciences, Delft University of Technology, Delft, the Netherlands

## ARTICLE INFO

### Keywords:

$C_3S$ -gypsum-slag system  
 $Al_2O_3$   
 Calorimetry measurement  
 Ettringite and calcium monosulfoaluminate  
 Sulfur rich species in slag  
 Thermodynamic modelling

## ABSTRACT

A deeper insight into  $SO_3/Al_2O_3$  ratio including the contribution of alumina in slag at early age is required to ensure a properly sulfated slag cement. In this paper, to investigate the effect of gypsum and alumina of slag, emphasis was laid on the hydration characteristics of  $C_3S$ -gypsum-slag system during the early age, of which slag was synthesized in the laboratory with varying  $Al_2O_3$  contents from 3.69 to 18.19 wt%.

The duration of dormant period during the hydration of  $C_3S$  depended on  $Al_2O_3$  content of slag significantly; however, the amount of silicate reaction before the onset of aluminate reaction was independent of slag chemistry and gypsum content added. The rate of aluminate reaction was controlled by the availability of reactants,  $SO_4^{2-}$  and  $Al^{3+}$  ions in particular, which were sourced from gypsum and slag, respectively. Calcium monosulfoaluminate only occurred in mixture when slag contained a high amount of  $Al_2O_3$  (18.19 wt% in this study) at early age, and its formation proceeded continuously at the expense of ettringite. Sulfur rich species incorporated in slag started to participate into aluminate reaction after the main hydration peak of  $C_3S$ , and it played a similar role to gypsum.

## 1. Introduction

Ordinary Portland cement (OPC) mainly consists of calcium silicate ( $C_3S$  and  $C_2S$ ), calcium aluminate ( $C_3A$  and  $C_4AF$ ) and calcium sulfate (Gypsum). Much attention has been paid to the hydration of its pure components, e.g.,  $C_3S$  (the major constituent),  $C_3A$  (the most reactive constituent), and usually with gypsum, in order to generate a fundamental understanding of the hydration process and performance of cement [1–6]. It is well recognized that the other two constituents,  $C_2S$  and  $C_4AF$ , contribute little at early age due to their relatively less reactive property. Moreover, gypsum or sulfate plays a key role in hydration through the reaction with  $C_3A$ , and affects the early age performance as a result [7]. Therefore, it is important to identify the optimum amount of gypsum added into the system.

Supplementary cementitious materials (SCMs) are widely used for partial cement replacement to lower the carbon dioxide footprint of concrete productions [8–11]. Meanwhile, blended cements necessitate the industry and academic to have a better understanding of sulfate requirement, rather than use the same gypsum addition in OPC system. J. Cheung et al. [12] found that SCMs added into cement resulted in an

undersulfated system, particularly in the presence of admixtures. Antoni et al. [13] elucidated that optimization of gypsum content in cement-calcined clay-limestone system increased one day compressive strength by >50%. On the other hand, an early depletion of sulfate and a rapid uncontrolled reaction between aluminate phase and gypsum was found in the mixture containing cement and Ca-rich aluminosilicate glass, of which high  $Al_2O_3$  content was observed in the glass [14]. Thus, a deep insight into  $SO_3/Al_2O_3$  ratio including the contribution of aluminate phase from SCMs is required to ensure a properly sulfated blended cement. However, results from [15] pointed out that it was the “filler effect” related to the specific surface area provided by SCMs, rather than the chemical composition, that exerted a significant effect on sulfate balance and dominated the higher sulfate requirement of cement-calcined clay-limestone system. Due to the “filler effect”, a faster precipitation of C–S–H gel phase resulted in an earlier consumption of gypsum because of absorption. After sulfate depletion, sulfate was desorbed from C–S–H gel phase and available to react with aluminate phases to form ettringite.

Blast furnace slag (slag for short), whose hydration needs activation, is a by-product from the production of pig iron and presents hydraulic

<sup>\*</sup> Corresponding author.

E-mail addresses: [Y.Zhang-28@tudelft.nl](mailto:Y.Zhang-28@tudelft.nl) (Y. Zhang), [Z.Wan-1@tudelft.nl](mailto:Z.Wan-1@tudelft.nl) (Z. Wan), [L.C.MirandadeLimaJunior@tudelft.nl](mailto:L.C.MirandadeLimaJunior@tudelft.nl) (L.M. de Lima Junior), [O.Copuroglu@tudelft.nl](mailto:O.Copuroglu@tudelft.nl) (O. Çopuroğlu).

<https://doi.org/10.1016/j.cemconres.2022.106954>

Received 4 June 2022; Received in revised form 12 August 2022; Accepted 17 August 2022

Available online 22 August 2022

0008-8846/© 2022 The Authors. Published by Elsevier Ltd. This is an open access article under the CC BY license (<http://creativecommons.org/licenses/by/4.0/>).

property. Blending cement with slag produces analogous hydrates compared with pure cement system. Portlandite, C–S(A)–H gel phase, ettringite, AFm phases, and a hydrotalcite-like phase are identified. According to [9,16], it is well accepted that slag chemistry changes considerably with time across the world, and the increasing or decreasing of  $\text{Al}_2\text{O}_3$  content in slag [17,18] thus upsets the hydrate assemblage in the blended cement, e.g., the distribution of aluminum in ettringite, AFm phases, and hydrotalcite-like phase. Moreover, it is still unknown whether or not this change will further affect sulfate balance in slag cement paste at early age. On the other hand, although  $\text{C}_3\text{S}$ – $\text{C}_3\text{A}$ –gypsum system has already been employed to investigate the sulfate balance of pure cement system [6,19], and the effect of  $\text{Al}_2\text{O}_3$  in SCMs on sulfate balance of blended cement system has also been noticed [12–15], the interaction among  $\text{C}_3\text{S}$ –( $\text{C}_3\text{A}$ )–slag–gypsum system at early age has not been reported specifically yet.

Therefore, the present research would like to get an insight into the interaction between aluminates and sulfate phases in cement–slag system at early age. Aluminate phases in the mixture come from two parts, one is  $\text{C}_3\text{A}$  in cement clinker and the other is  $\text{Al}_2\text{O}_3$  in slag. Sulfate phases mainly originate from gypsum added in the cement, and a small amount also sources from sulfur rich species in slag, which will transform into sulfate eventually in an alkaline environment [20–22]. Model cement–slag system containing 30 wt%  $\text{C}_3\text{S}$  + ( $\text{C}_3\text{A}$ ) + gypsum and 70 wt% slag was used throughout the research to simulate CEM III/B and highlight the effect of  $\text{Al}_2\text{O}_3$  in slag. In this paper, the authors laid emphasis on the hydration characteristics of  $\text{C}_3\text{S}$ –gypsum–slag system at early age (until 3 days) firstly. To specify the effect of  $\text{Al}_2\text{O}_3$  and sulfur rich species in slag, one commercial slag incorporating sulfur and three synthetic slags with varying  $\text{Al}_2\text{O}_3$  contents from 3.69 to 18.19 wt% but without sulfur were employed. In our next publication, analytically reagent  $\text{C}_3\text{A}$  would be incorporated, and the agreement and disagreement with real slag cement paste would be analyzed. Apparently, the results found in this paper and following publication can provide new prospects to understand the interaction among  $\text{C}_3\text{S}$ ,  $\text{C}_3\text{A}$ , slag, and gypsum in slag cement at early age. Additionally, it also contributes to understanding the role of  $\text{Al}_2\text{O}_3$  in slag and its effect on  $\text{SO}_3/\text{Al}_2\text{O}_3$  ratio.

## 2. Material and methodology

### 2.1. Material

One commercial slag (S) provided by Ecocem Benelux B.V., three synthetic slags (A3, A12, A18) with different  $\text{Al}_2\text{O}_3$  contents, and quartz (QZ) acting as reference were used in the study. Their chemical compositions determined by XRF are presented in Table 1. The particle size distribution (PSD) of slags and quartz was measured by laser diffraction and is shown in Fig. 1.

The synthetic slags used in the present research were prepared by mixing commercial slag S with AR (analytical reagent) CaO, MgO,  $\text{SiO}_2$ ,  $\text{Al}_2\text{O}_3$  according to different design targets. The commercial slag S and analytical reagents added to control the exact composition in each run were mixed into a homogeneous blend by combining the materials with pure ethyl alcohol, grinding the mixture in a ball milling machine at a low speed for 2 h and drying them at  $100^\circ\text{C}$  for 24 h. The dried sample paste was then ground to  $<200\ \mu\text{m}$  in a mortar for better homogeneity. Then, it was melted in an  $\text{Al}_2\text{O}_3$  crucible at  $1550^\circ\text{C}$  in the oven for 3 h (heated from room temperature to  $1550^\circ\text{C}$  at a rate of  $10^\circ\text{C}/\text{min}$  and maintained at  $1550^\circ\text{C}$  for 3 h). The molten liquid was water quenched to obtain glassy slag, rinsed with isopropanol and dried at  $100^\circ\text{C}$  for 24 h subsequently. Finally, it was crushed and ground to required particle size distribution. For synthetic slag A3, A12 and A18, the CaO/ $\text{SiO}_2$  ratios were maintained at approximately 1 and the amounts of MgO stabilized at about 9 wt%, while  $\text{Al}_2\text{O}_3$  contents increased from 3.69 (A3) to 18.19 wt% (A18). In other words, the  $\text{Al}_2\text{O}_3$  content increased with the decreasing of CaO and  $\text{SiO}_2$  contents simultaneously.

Analytically reagent  $\text{C}_3\text{S}$  and gypsum ( $\text{CaSO}_4\cdot 2\text{H}_2\text{O}$ ) were also

**Table 1**

Chemical compositions (wt%) determined by XRF and physical properties of these slags.

	A3	A12	A18	S
CaO	42.07	37.32	36.87	37.40
$\text{SiO}_2$	43.30	39.11	34.43	37.82
$\text{Al}_2\text{O}_3$	3.69	12.32	18.19	13.58
MgO	10.83	9.43	7.98	8.11
$\text{FeO}/\text{Fe}_2\text{O}_3$	0.07	0.30	0.40	0.36
$\text{TiO}_2$	–	0.70	0.84	1.22
$\text{MnO}/\text{Mn}_2\text{O}_3$	–	0.15	0.27	0.30
$\text{Na}_2\text{O}$	–	0.24	0.37	–
$\text{K}_2\text{O}$	–	0.21	0.41	0.80
$\text{SO}_3$	0.01	0.03	0.03	0.93
LOI <sup>a</sup>	–0.02	–0.03	–0.04	–0.87
Physical properties				
$d_{50}$ ( $\mu\text{m}$ ) <sup>b</sup>	19.67	20.35	20.85	20.94
SSA ( $\text{m}^2/\text{g}$ ) <sup>c</sup>	1.090	0.919	0.904	0.937

<sup>a</sup> The loss-on-ignition (LOI) of slags was determined by thermogravimetric analysis at  $950 \pm 50^\circ\text{C}$ . The negative value of LOI is related to the oxidation of sulfur rich species in slag. It should be noted that the LOI value was not corrected in the XRF measurement.

<sup>b</sup> The particle size distribution of slag was measured by EyeTech, Ankersmid. The  $d_{50}$  of quartz is  $24.21\ \mu\text{m}$ .

<sup>c</sup> The specific surface area (SSA) of slag was measured by nitrogen adsorption with the BET method.

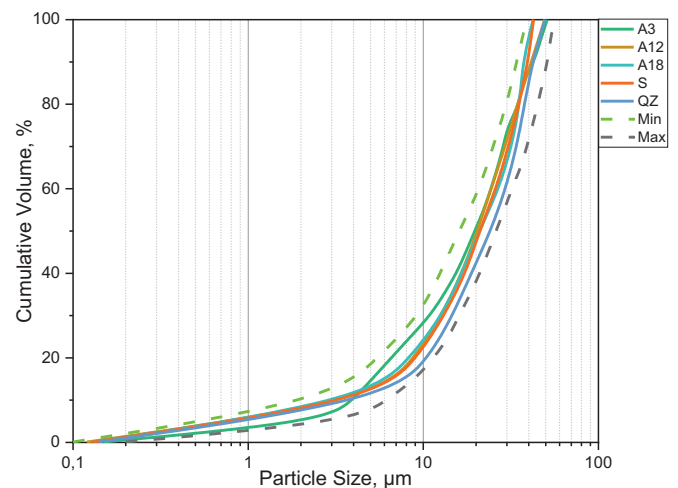


**Fig. 1.** Particle size distribution of slags and quartz.

employed to prepare  $\text{C}_3\text{S}$ –gypsum–slag system. A representative X-ray diffraction (XRD) result of  $\text{C}_3\text{S}$  is shown in Fig. 2(a), and the result indicated that it presented a triclinic polymorph. Fig. 2(b) elaborates the XRD scans of these four slags, showing that they were entirely amorphous with no obvious crystal peak.

### 2.2. Mix design and experimental method

A summary of the specimens prepared for investigation is listed in Table 2. The slag to  $\text{C}_3\text{S}$  or  $\text{C}_3\text{S}$  + gypsum ratio was 7/3 and the water to binder ratio was 0.4. Sulfate sourcing from gypsum was introduced by replacing  $\text{C}_3\text{S}$ . Each mixture was labelled as their corresponding sulfate content levels, i.e., G0, G1, G3, G5, and G10 for sulfate dosage levels of 0, 1, 3, 5, and 10 wt% of  $\text{C}_3\text{S}$  + gypsum, respectively.

The heat evolution was measured in a TAM Air isothermal calorimeter at  $20^\circ\text{C}$ . Sample was mixed at a high speed for 2 min,  $\sim 7\ \text{g}$  of the binder was transported to a glass ampoule, sealed and placed in the calorimeter. Paste specimen was prepared in the same manner as the

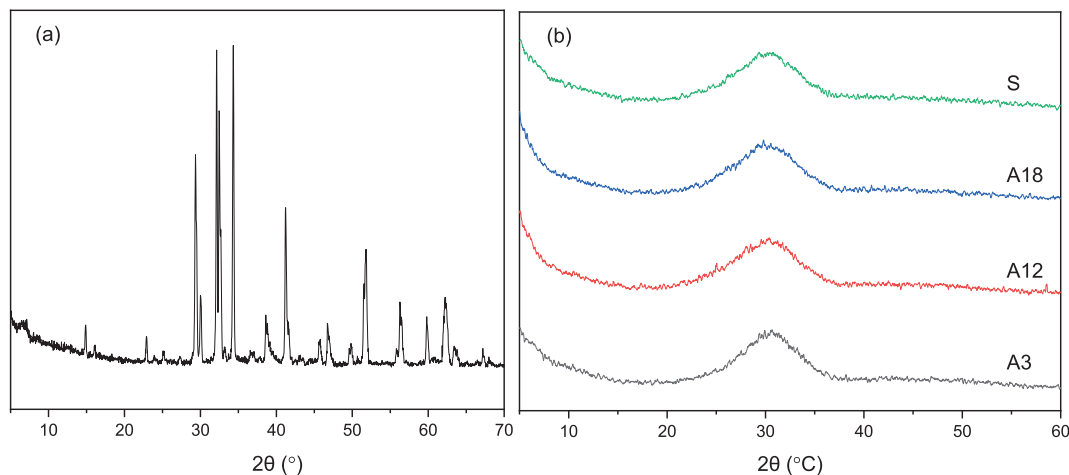


Fig. 2. XRD scan of (a)  $C_3S$  and (b) one commercial slag and three synthetic slags used in the present research.

Table 2

Compositions (wt%) of the blends.

	$C_3S$	Gypsum	Slag	$SO_3/(C_3S + \text{gypsum})$	Slag/ $(C_3S + \text{gypsum})$
G0	30	0	70	0	7/3
G1	29.355	0.645	70	1 %	7/3
G3	28.065	1.935	70	3 %	7/3
G5	26.775	3.225	70	5 %	7/3
G10	23.550	6.450	70	10 %	7/3

calorimetry measurement, mounted in the plastic bottle of 20 mL and sealed with thin para film on the seal to avoid any ingress of carbon dioxide and evaporation of vapor. Sealed curing was performed for all specimens at  $20 \pm 3$  °C for 1 day and 3 days before any measurements.

For XRD measurement and thermogravimetric analysis (TGA), the continuous hydration of specimen was stopped by solvent exchange with isopropanol. Slices of specimen were cut, crushed, and ground to below 63  $\mu\text{m}$ . X-ray powder diffraction was performed on a Philips PW 1830/40 Powder diffractometer employing the Cu K-alpha radiation. The machine was operated with an acceleration voltage of 40 kV and an X-ray beam current of 40 mA. Analysis was performed with a step size of  $0.03^\circ$  and for a  $2\theta$  range from  $5^\circ$  to  $60^\circ$ . Thermogravimetric analysis was carried out by Netzsch STA 449 F3 Jupiter under Argon atmosphere. Approximately 50 mg of the material was heated from 40 to 900 °C with a heating rate of 10 °C/min in an  $Al_2O_3$  crucible with an identical

crucible as reference.

Meanwhile, the fresh fracture surface of specimen was observed with a FEI QUANTA FEG 650 ESEM in secondary electron (SE) mode after hydration stop. Moreover, the overall development of microstructure was observed on the polished surface in backscattered electron (BSE) mode. To get BSE images, slices of hydrated specimen were cut, immediately immersed in isopropanol solution for hydration stop, dried at 40 °C subsequently, impregnated with epoxy resin and polished down to 0.25  $\mu\text{m}$ . X-ray energy dispersive (EDS) detector was used to determine the elemental composition of hydrate assemblage. All microanalysis was carried out in high vacuum chamber condition at a working distance of 10 mm and an accelerating voltage of 15 kV.

### 3. Results and discussions

#### 3.1. General pattern of the reaction of $C_3S$ -gypsum-slag system

Fig. 3 illustrates the heat flow and heat release of  $C_3S$ -5 wt% gypsum-slag system (G5), normalized to per gram of  $C_3S$ . The heat flow was dominated by one main peak occurring at about 10 h after mixing, associated with the hydration of  $C_3S$ , and followed by a hump after 1 day (labelled A), which was affected by the amount of  $Al_2O_3$  in slag and gypsum content added. This hump was indicative of secondary reaction between  $Al^{3+}$  ion from slag and  $SO_4^{2-}$  ion from gypsum.

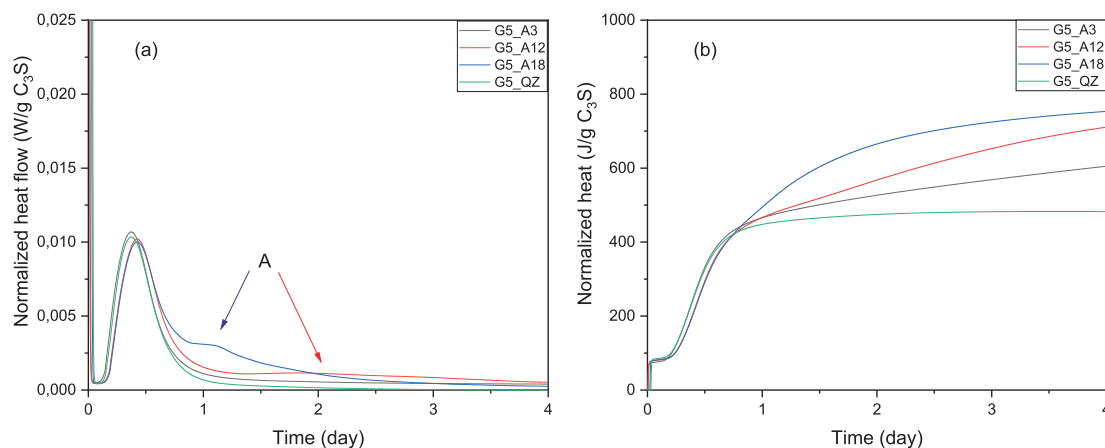


Fig. 3. (a) Heat flow and (b) total heat release as a function of time in calorimetric measurement for  $C_3S$ -5 wt% gypsum-slag system. As seen in (b), the heat release before 1 day was almost the same irrespective of the  $Al_2O_3$  content of slag.

### 3.1.1. Effect of $Al_2O_3$ in slag

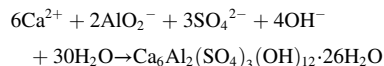
It is well recognized that  $Al^{3+}$  ion has a perturbing effect on the reactivity of silicate [23–27], relying mainly on aluminate concentration and pH of the solution [26,27]. As seen in the present research (Fig. 4 (a)), when increasing  $Al_2O_3$  content in slag, the induction period became longer, implying a rough dependence on alumina dosage. Surface poisoning is believed to take place either through covalent bonding between alumina and silicate on the surface or through the adsorption of alumina on the etch pits [27]. Another mechanism that has been put forward is the negative effect of alumina on the nucleation and growth of silicate hydrates [6,28]. Moreover, compared with  $C_3S$ -quartz blend, a small decrease in the rate of heat flow (slope) during acceleration period and the intensity of main hydration peak was observed, with the presence of alumina. The more  $Al_2O_3$ , the more drop. It was in contrast with the results from [29], which concluded that the intensity of main peak and total heat release increased with increasing  $Al^{3+}$  ion concentration, indicating a higher hydration degree of  $C_3S$ . On the other hand, the deceleration period appeared to be unaffected by the presence of  $Al_2O_3$ .

### 3.1.2. Effect of gypsum

As shown in Fig. 4(b), gypsum itself seemed to exert few impact on the hydration of  $C_3S$  when compared in  $C_3S$ -quartz-gypsum mixture. The rate of heat flow during acceleration and deceleration period was nearly the same when different amounts of gypsum were added, except for a small variation of the main peak intensity. It was consistent with the results from [6], where the reaction rate of  $C_3S$  with or without gypsum addition was almost identical. Additionally, the dormant period ended a little earlier with gypsum, indicating that  $SO_4^{2-}$  ion increased the deviation of  $C_3S$  from the solubility equilibrium, and its dissolution was accelerated accordingly [26].

### 3.1.3. Effect of $Al_2O_3$ and gypsum together

It was different when slag and gypsum were added together into the system. As seen in Fig. 5(a), for  $C_3S$ -gypsum-slag A3 system, the hydration process was accelerated, proved by the shortened induction period even compared with  $C_3S$ -quartz blend.  $Al^{3+}$  ion absorbed on the reactive site of  $C_3S$  was removed by  $SO_4^{2-}$  ion immediately, and as mentioned earlier, the rest  $SO_4^{2-}$  ion increased the deviation of  $C_3S$  from the solubility equilibrium. The hydration of  $C_3S$  was thus accelerated. Besides, it should be noted that the interaction between  $Al^{3+}$  and  $SO_4^{2-}$  ions led to the formation of ettringite through the equation below. Its precipitation decreased the concentration of  $Ca^{2+}$  in the pore solution, and increased the undersaturation levels with respect to C–S–H gel phase and portlandite. Therefore,  $C_3S$ -gypsum-slag A3 system entered into acceleration period firstly.



Similarly, for  $C_3S$ -gypsum-slag A12 and A18 systems, the induction period also ended earlier than  $C_3S$ -slag A12 and A18 systems without gypsum, but a little later than  $C_3S$ -quartz blend (Fig. 5(b) and (c)). When increasing gypsum addition from 1 to 10 wt%, it made few differences. Apparently, the  $Al^{3+}$  concentrations in the pore solution of slag A12 and A18 were higher than that in slag A3 due to their higher  $Al_2O_3$  contents in slag. Probably  $SO_4^{2-}$  ion provided by gypsum cannot combine all  $Al^{3+}$  ion absorbed on the  $C_3S$  surface in time, and residual  $Al^{3+}$  ions were still absorbed on the  $C_3S$  surface. For this phenomenon, it deserves further research.

### 3.2. Second reaction peak (aluminate peak)

For pure cement system, the second reaction peak originates from the renewed reaction between  $C_3A$  and sulfate, and the work in [8,30] found that the peak was delayed and became broader with increasing additional gypsum content. Also, this peak may not be well visible in the calorimetry curve as it is often present as a low and broad peak. Nonetheless, this peak occurred in  $C_3S$ -gypsum-slag mixture in the present research with the absence of  $C_3A$  (see Fig. 6), and was associated with the  $Al_2O_3$  content of slag and gypsum content added remarkably.

In a properly sulfated cement system, the second aluminate peak in calorimetry measurement occurs right after the main hydration peak. All the mixtures investigated in the article belong to this case. However, in a undersulfated system, a large and sharp peak, related to the formation of calcium monosulfoaluminate (monosulfate for short), occurs much earlier before the main hydration peak, and the reaction of  $C_3S$  is delayed and suppressed [6,31]. This is not the case in the present research even with only 1 wt% gypsum addition (G1) owing to the reactivity of slag, which is much inferior to  $C_3A$ . As for oversulfated system, more retardation on the reaction of  $C_3A$  can be observed [4].

#### 3.2.1. Parameters controlling the hydration kinetics of aluminate reaction

As Fig. 6(a) illustrates, after the main hydration peak, the heat evolution was featured by a period when the reaction was accelerated to a small peak and then slowed down, especially for those with high gypsum addition. The second reaction peak in  $C_3S$ -gypsum-slag A18 system started to be visible when 5 wt% gypsum was added and a little delayed when increasing gypsum content from 5 to 10 wt%.

It was also noticed that the onset of aluminate peak (beginning of the deviation from  $C_3S$ -quartz blend) occurred at a similar timing ( $\sim 15$  h after mixing as Fig. 6(a) presents) or cumulative heat release ( $\sim 400$  J/g

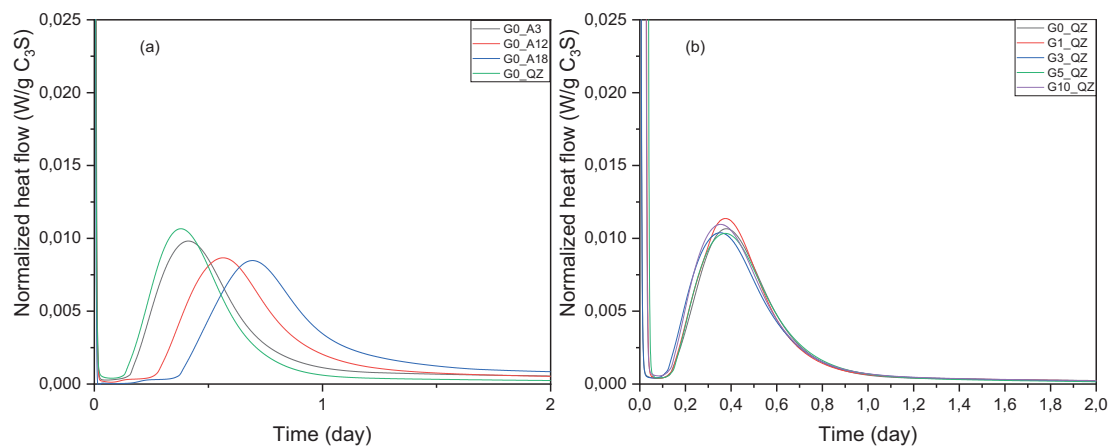
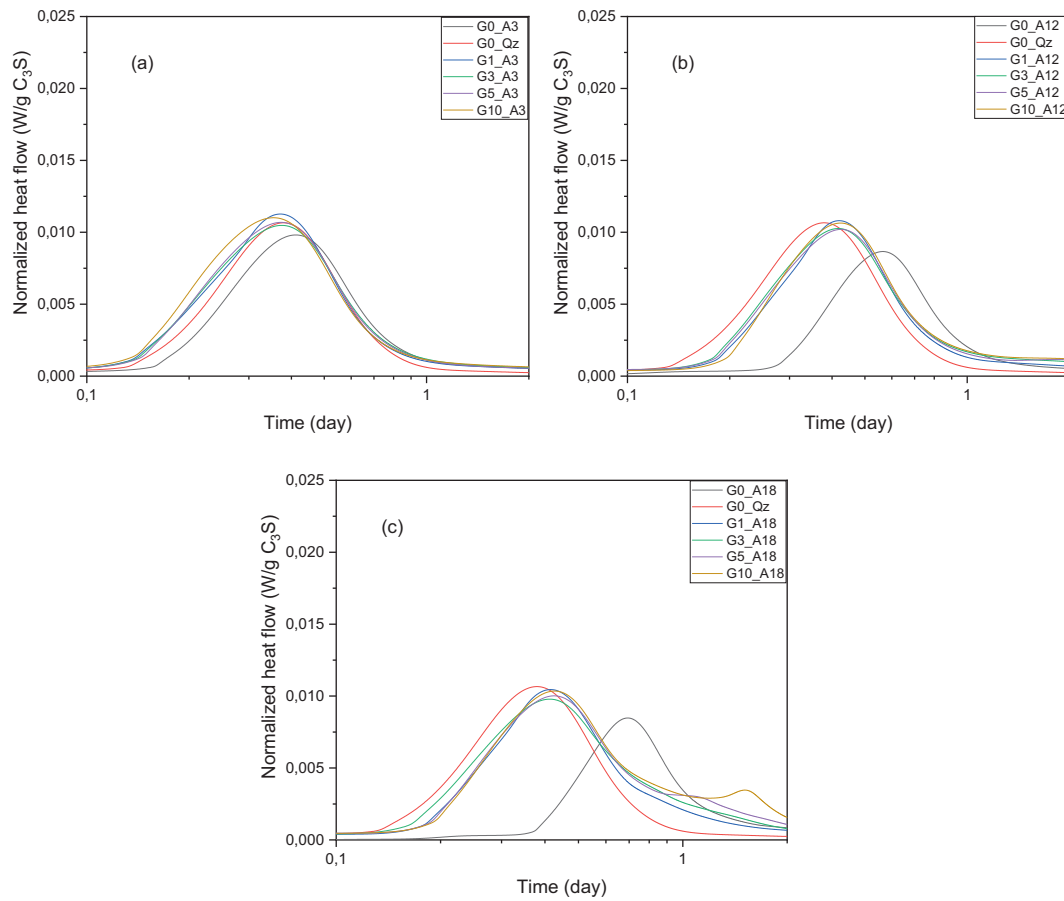
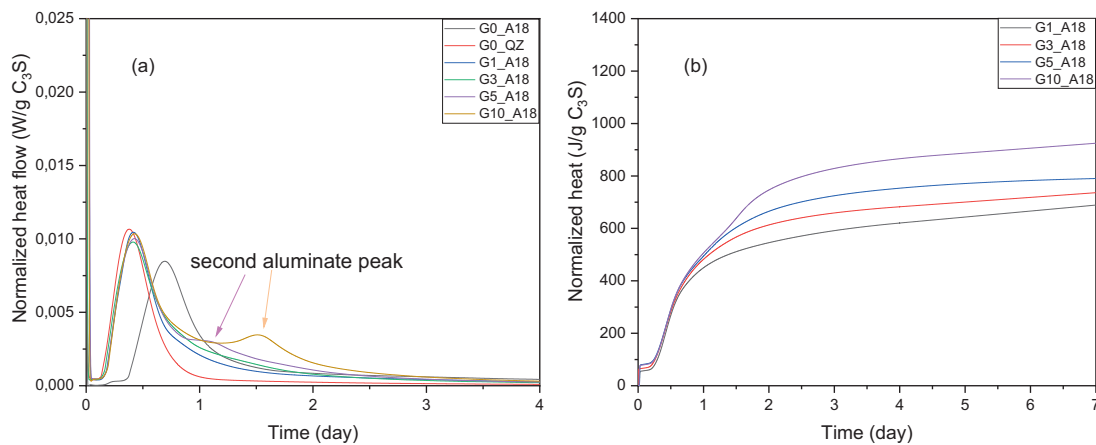


Fig. 4. (a) The dormant period or the nucleation of  $C_3S$  was strongly modified in the presence of slag containing different  $Al_2O_3$  contents. (b) The reaction rate of pure  $C_3S$  with or without gypsum addition was almost identical.



**Fig. 5.** Calorimetric curves of C<sub>3</sub>S-slag blend with different gypsum additions. (a) The addition of gypsum promoted the earlier end of induction period in C<sub>3</sub>S-slag A3 blend compared with C<sub>3</sub>S-quartz blend; As for C<sub>3</sub>S-gypsum-slag A12 (b) and A18 (c) systems, the induction period ended a little later than C<sub>3</sub>S-quartz blend. These curves were plotted on log scale to highlight the difference at early age.



**Fig. 6.** Calorimetric curves of C<sub>3</sub>S-slag A18 blend with different gypsum additions. (a) The aluminate peak was delayed, and became more visible with the increasing gypsum addition; (b) The normalized heat release curves were almost identical before ~15 h (about ~400 J/g C<sub>3</sub>S) after mixing, and they separated from each other from then on.

C<sub>3</sub>S) as Fig. 6(b) presents) for all mixtures irrespective of the amount of gypsum added. The heat was mainly released by silicate reaction until this timing, i.e., the hydration of C<sub>3</sub>S, which suggested that the onset of aluminate reaction also depended on silicate reaction, perhaps the production of enough C–S–H gel phase to absorb sulfate. Zunino, F. et al. [19] concluded that the heat release before aluminate peak was directly related to the content of gypsum added and the fineness of C<sub>3</sub>A,

in other words, it was determined by the amount of silicate reaction and ettringite formation. In the present research where there was no C<sub>3</sub>A in the mixture, the almost same heat release before aluminate peak demonstrated that the precipitation of ettringite was very few even in G10\_A18 mixture. It proved indirectly that SO<sub>4</sub><sup>2-</sup> ions cannot combine all Al<sup>3+</sup> ions absorbed on the C<sub>3</sub>S particle surface during the induction period (Section 3.1.3).



For systems with lower  $\text{Al}_2\text{O}_3$  content in slag, this period was almost invisible (slag A3 in Fig. 7(a)) or characterized by a hump (slag A12 in Fig. 7(b)). Therefore, it was assumed that the aluminate reaction was controlled by the availability of reactants,  $\text{SO}_4^{2-}$  and  $\text{Al}^{3+}$  ions in particular for the formation of ettringite. Nuclei of ettringite precipitate and grow at a rate proportional to the concentrations of  $\text{SO}_4^{2-}$  and  $\text{Al}^{3+}$  ions [32,33].

Fig. 8(a) presents the normalized heat release of  $\text{C}_3\text{S}$ -gypsum-slag A3 system until 4 days with different gypsum additions. The shape of curve was analogous to each other and the difference of total heat release was very small among each other. Hence it was convincible to conclude that the amount of gypsum added was adequate to react with  $\text{Al}^{3+}$  ion in each mixture, and the availability of  $\text{Al}^{3+}$  ion was the rate-controlling factor. Fig. 8(b) and (c) illustrate the normalized heat release of  $\text{C}_3\text{S}$ -3 and 5 wt % gypsum-slag systems (G3 and G5). It was noted that although the total heat releases of slag A12 and A18 mixtures were different until 4 days, it coincided with each other after 7 days of curing. It implied that the same amount of reaction occurred in slag A12 and A18 mixtures until 7 days, whereas the kinetics were different and affected by the availability of reactants. There seemed to be abundant  $\text{Al}^{3+}$  ions in these two mixtures to participate into the aluminate reaction. Thus, the availability of  $\text{SO}_4^{2-}$  ion was the rate-controlling factor for slag A12 and A18 systems when gypsum addition was <5 wt%. Fig. 8(d) shows the normalized heat release of  $\text{C}_3\text{S}$ -10 wt% gypsum-slag system (G10) until 7 days. The difference of total heat release between slag A12 and A18 mixtures became evident, indicating that  $\text{SO}_4^{2-}$  ion was sufficient in the pore solution and the availability of  $\text{Al}^{3+}$  ion dominated the reaction again. The rate-controlling factor of aluminate reaction in each run is summarized in the Table 3.

Moreover, it was noticed that all cumulative heat release curves deviated from each other at a similar timing, i.e., ~15 h after mixing or ~400 J/(g  $\text{C}_3\text{S}$ ) as displayed from Fig. 8(a) to (d). The same heat release before the onset of aluminate peak further confirmed that the precipitation of ettringite was few in all mixtures, irrespective of alumina content in slag. On the other hand, it indicated that the dissolution degree of slag before one day was very low, and the surface area of slag could be considered to be unchanged at this stage. After one day, slag, especially with high alumina content, could not be regarded as inert filler any more, and it took part into the aluminate reaction with gypsum significantly.

Another aspect needed to be emphasized was the location where ettringite grew, on the surface of  $\text{C}_3\text{S}$  particle, slag particle or in the pore solution. Firstly, it was unlikely for ettringite to nucleate and grow on the surface of  $\text{C}_3\text{S}$  particles as their surface had been occupied by C-S-H gel phase after main hydration peak (Fig. 15). Moreover, as Fig. 14 shows, these needle-like ettringite was more likely to grow from

the pore solution with an exclusive through-solution formation, as reported in [32].

### 3.2.2. Heat release from aluminate reaction vs. $\text{SO}_3$ and $\text{Al}_2\text{O}_3$ contents of the mixture

Fig. 9(a) and (b) display the heat release from aluminate reaction against  $\text{SO}_3$  content of gypsum and  $\text{Al}_2\text{O}_3$  content of slag, respectively. An approximatively linear correlation between  $\text{SO}_3$  content and heat release from aluminate reaction, taken as an indication of the amount of ettringite formed, is found and depicted in Fig. 9(a). A linear function was selected for fitting, and its parameters were determined by the least-square method considering all points investigated. For slag A3 and A12 systems, slopes were in direct proportion to their corresponding  $\text{Al}_2\text{O}_3$  contents, while for slag A18 system, the slope was a little higher compared to its  $\text{Al}_2\text{O}_3$  content, i.e.,  $3.75/3.69 \approx 10.99/12.32 < 23.51/18.19$ . The roughly linear correlation was also found between  $\text{Al}_2\text{O}_3$  content of slag and heat release in most mixtures investigated (Fig. 9(b)), except for  $\text{C}_3\text{S}$ -10 wt% gypsum-slag A18 mixture, which presented a significant high heat release from aluminate reaction. Unlike alumina in slag A3 and A12 systems only participating into the formation of ettringite, aluminum dissolved from slag A18 played role both in the formation of ettringite and monosulfate (see discussion in Section 3.3.1). The heat evolved from the transformation from ettringite to monosulfate in slag A18 mixture was also included in the aluminate reaction without differentiation. As a result, more heat and higher slope were determined in this mixture.

### 3.2.3. Effect of sulfur rich species of slag

The sulfur rich species of slag mainly sources from iron pyrite used as raw material and fuel for energy. It exists as anion  $\text{S}^{2-}$  in the molten slag liquid due to the reduction condition in the blast furnace [34,35]. During quenching, it will be emitted in the form of  $\text{H}_2\text{S}$  with water vapor. The rest exists as sulfide (e.g., CaS) in slag, whereas its amount is presented in the form of  $\text{SO}_3$  by XRF. In the pore solution of slag cement paste, dissolved  $\text{S}^{2-}$  ion could be readily oxidized depending on oxygen diffusion into pores through thiosulfate ( $\text{S}_2\text{O}_3^{2-}$ ) to most stable sulfate ( $\text{SO}_4^{2-}$ ) [36,37].

As shown in Fig. 10, it was found that the sulfur rich species incorporated in commercial slag exerted a key impact on the hydration of  $\text{C}_3\text{S}$ -slag S blend when without gypsum addition. On the one hand, the dormant period ended earlier in  $\text{C}_3\text{S}$ -slag S mixture compared with that in  $\text{C}_3\text{S}$ -slag A12 mixture (Slag A12 contained nearly no sulfur (see LOI value in Table 1)). In addition, the heat flow curve of  $\text{C}_3\text{S}$ -slag S mixture was almost identical with that of  $\text{C}_3\text{S}$ -3 wt% gypsum-slag A12 mixture, especially for the similar duration of induction period. It suggested that the sulfur species in slag S acted the same role as sulfate dissolved from

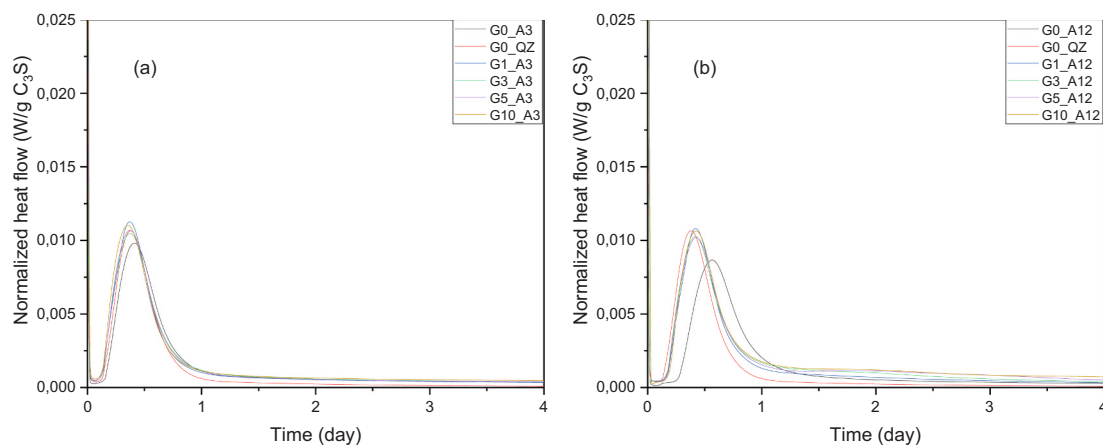
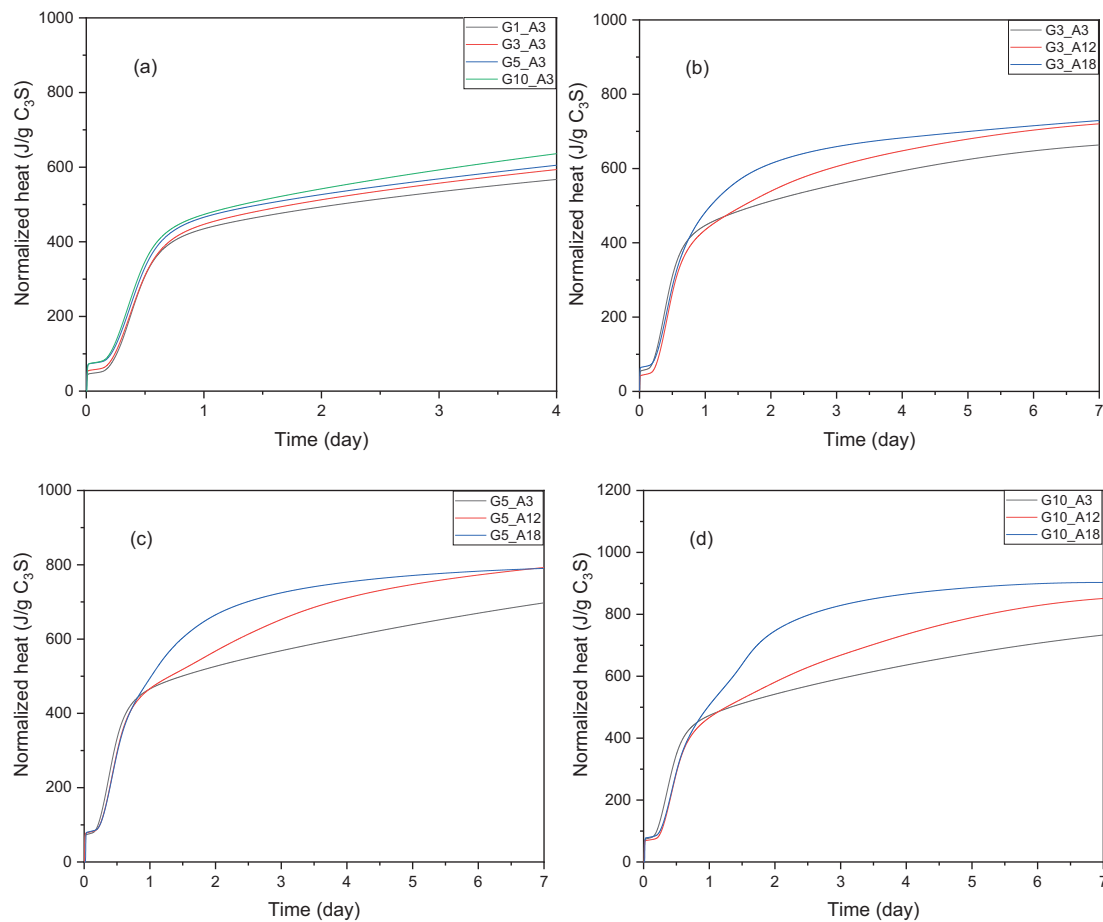


Fig. 7. Calorimetric curves of  $\text{C}_3\text{S}$ -slag (a) A3 and (b) A12 blends with different gypsum additions. The aluminate peak was invisible in slag A3 system or characterized by a hump in slag A12 system.



**Fig. 8.** (a) Heat release of  $C_3S$ -gypsum-slag A3 system and the availability of  $Al^{3+}$  ion in the pore solution was the rate-controlling factor in this system; (b) and (c) Heat release of  $C_3S$ -3 and 5 wt% gypsum-slag systems respectively, and there seemed to be abundant  $Al^{3+}$  ions to participate into the aluminate reaction and the availability of  $SO_4^{2-}$  ion was the rate-controlling factor; (d) Heat release of  $C_3S$ -10 wt% gypsum-slag system and the availability of  $Al^{3+}$  ion dominated the reaction again as  $SO_4^{2-}$  ion was sufficient in the pore solution.

**Table 3**

The rate-controlling factor of aluminate reaction in each run, the availability of  $Al^{3+}$  or  $SO_4^{2-}$  ion.

	A3	A12	A18
G1	$Al^{3+}$	$SO_4^{2-}$	$SO_4^{2-}$
G3	$Al^{3+}$	$SO_4^{2-}$	$SO_4^{2-}$
G5	$Al^{3+}$	$SO_4^{2-}$	$SO_4^{2-}$
G10	$Al^{3+}$	$Al^{3+}$	$Al^{3+}$

gypsum, and  $Al^{3+}$  ion absorbed on the reactive site of  $C_3S$  would be removed by  $SO_4^{2-}$  ion transformed from sulfur species. On the other hand, the hump (labelled as A) indicating the reaction between  $Al^{3+}$  and  $SO_4^{2-}$  ions for the formation of ettringite was also noted in the  $C_3S$ -slag S mixture.

To semi-quantify the effect of sulfur species incorporated in commercial slag S, calorimetric measurement of  $C_3S$ -slag A12 and S systems with different gypsum additions is compared in Fig. 11. The duration of induction period, the rate of heat flow during acceleration and deceleration period, and the occurrence of main hydration peak were nearly the same in these mixtures, except for a small variation of the main hydration peak intensity (Fig. 11(a)). As for the cumulative heat release, it was noted that  $C_3S$ -3 and 5 wt% gypsum-slag A12 mixtures presented almost the same heat as  $C_3S$ -1 and 3 wt% gypsum-slag S mixtures up to 4 days, respectively. In other words, about 2 wt% of gypsum was added into the blend by commercial slag S additionally through sulfur rich species.

### 3.3. Hydration products

#### 3.3.1. Solid phase

DTG results of typical mixtures are displayed in Fig. 12. The main hydrates formed in the mixture without gypsum were similar (Fig. 12(a)). The mass loss from 400 to 500 °C was sourced from the dehydration of portlandite. Hydrotalcite-like phase can also be detected (mass loss at around 350 °C). The mass loss at ~150 °C indicated the presence of C-S-H gel phase. More hydrates were identified with hydration, and compared with  $C_3S$ -quartz mixture, more C-S-H gel phase while less portlandite were detected in  $C_3S$ -slag mixture as part of portlandite and slag was consumed in pozzolanic reaction for the secondary precipitation of C-S-H gel phase and hydrotalcite-like phase.

For  $C_3S$ -gypsum-slag system (Fig. 12(b)), apart from phases identified earlier, ettringite was observed as the peak at ~150 °C became narrow and shifted left a little bit (Fig. 12(c)). Furthermore, monosulfate occurred in slag A18 mixture from the first day. Compared with  $C_3S$ -gypsum 5 wt%-slag A3 paste, slag A18 paste produced more ettringite + C-S-H gel phase and monosulfate (only visible in slag A18 paste) after 3 days of curing. Meanwhile, less portlandite was identified in slag A18 mixture due to its consumption in the formation of ettringite with gypsum and transformation from ettringite to monosulfate.

XRD scans (Fig. 13) reveal the presence of portlandite and unhydrated  $C_3S$  in the pastes. For C-S-H gel phase, the main peaks are located at ~30° (2θ) (PDF 34-0002 and PDF 34-0306), which is very difficult to distinguish from that of  $C_3S$ . It was also evidenced that monosulfate started to be detected in slag A18 paste containing gypsum



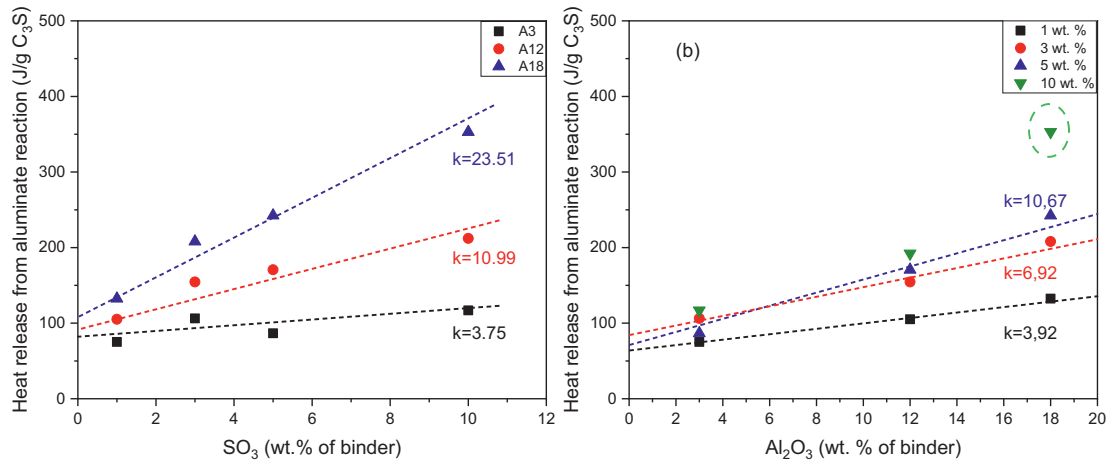


Fig. 9. Heat release from aluminate reaction against (a)  $\text{SO}_3$  content of gypsum and (b)  $\text{Al}_2\text{O}_3$  content of slag.

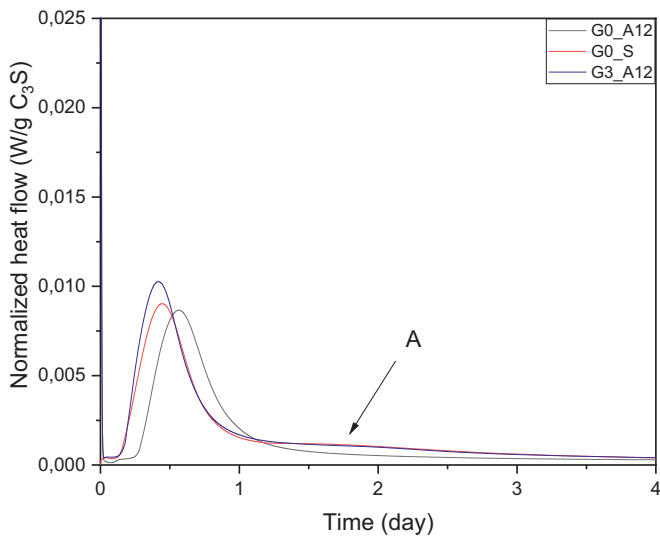


Fig. 10. Heat flow as a function of time in calorimetric measurement for  $\text{C}_3\text{S}$ -slag A12 and S systems.

from the first day (Fig. 13(c)), and the transformation from ettringite to monosulfate proceeded continuously with hydration. It deserved to mention that there was no monosulfate detected either by TGA or XRD in  $\text{C}_3\text{S}$ -gypsum 5 wt%-slag A3 and A12 systems.

3.3.2. Microstructure

Fig. 14 illustrates the representative BSE image of  $\text{C}_3\text{S}$ -5 wt% gypsum-slag A18 system after 3 days of curing. The mixture of anhydrous materials, hydrated phases and pores was clearly visible. Small  $\text{C}_3\text{S}$  grains, or so-called Hadley grains, hydrated completely after 3 days to leave hollow hydration shells (circled and labelled as 1). Large  $\text{C}_3\text{S}$  grains continued to hydrate, and there was a clear grey level difference between the outer products (Op) appearing dark grey, and more dense products (Ip) appearing light grey around unhydrated  $\text{C}_3\text{S}$  particle (circled and labelled as 2). Mass of ettringite (long needle shape) was observed frequently and crystallized in or near pores. Monosulfate only existed in slag A18 paste as fine and compact crystal intermixed with C-S-H gel phase (circled and labelled as 3). Although slag hydrated slowly, the formation of hydrates around unhydrated slag particles were observed (circled and labelled as 4).

Fig. 15(a) and (b) display the morphology of hydrates in  $\text{C}_3\text{S}$ -slag A12 mixture without gypsum at 3 days, where (a) clearly elaborates the precipitation of C-S-H gel phase and portlandite on the surface of slag particle. As shown in (b), hexagonal thin plates of portlandite were identified intermixed with C-S-H gel phase closely. It was also noticed that converging needles rather than a divergent fibrillary-like structure

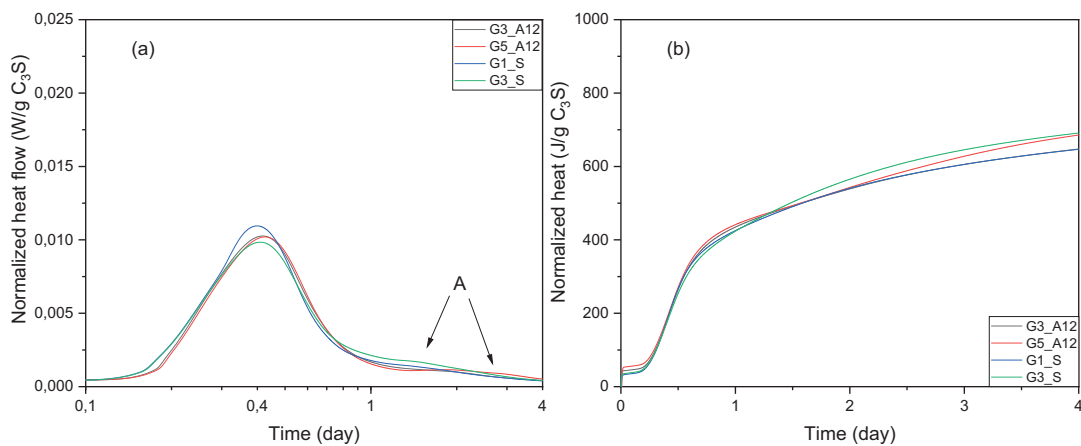
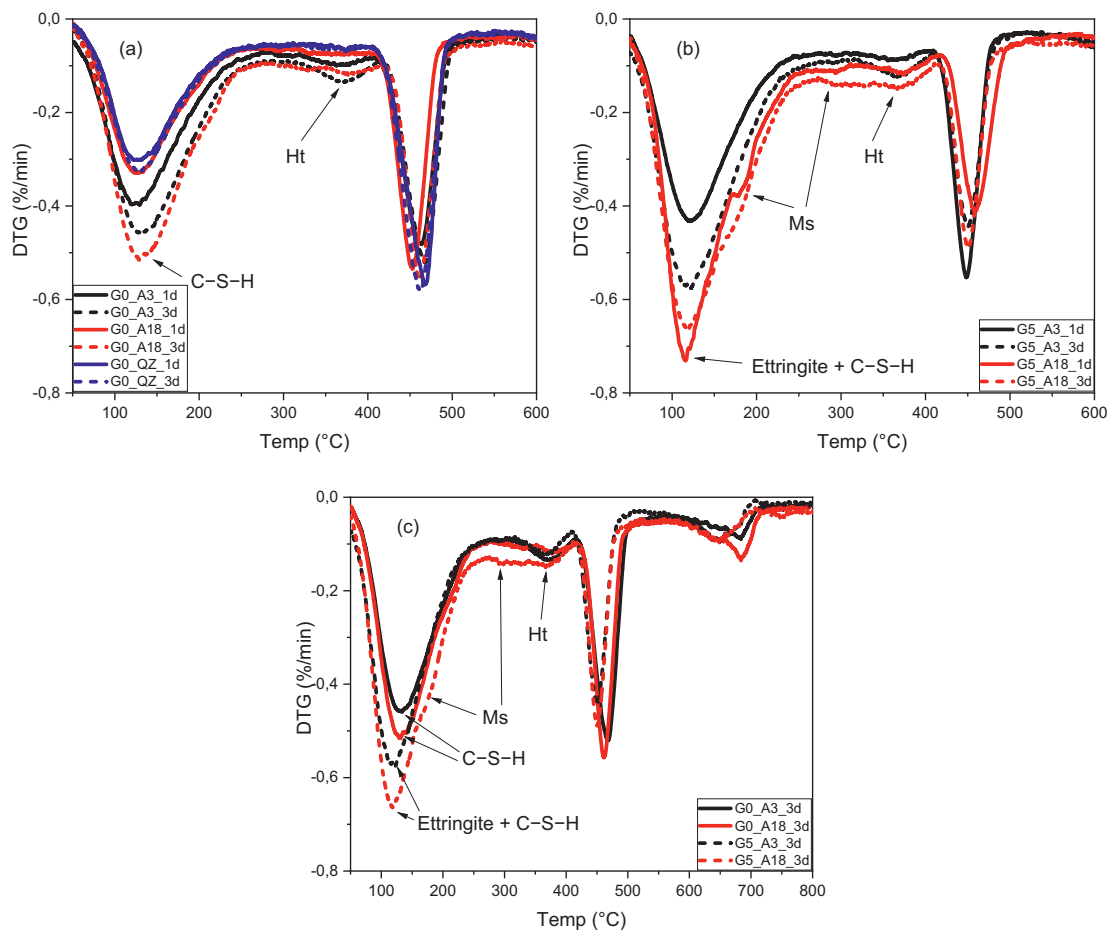


Fig. 11. (a) Heat flow and (b) total heat release as a function of time in calorimetric measurement for  $\text{C}_3\text{S}$ -slag A12 and S systems with different gypsum additions. (a) was plotted on log scale.



**Fig. 12.** Exemplary results of DTG analysis of paste (a) without gypsum and (b) with gypsum after 1 and 3 days of curing; (c) comparison between them. Ms: calcium monosulfoaluminate; Ht: hydrotalcite-like phase.

of C–S–H gel phase was seen in mixtures without gypsum at the very beginning of reaction. It was consistent with the results in [38], which confirmed that it was the pore solution chemistry, like the existence of  $\text{SO}_4^{2-}$  ion, changed the morphology of C–S–H gel phase by promoting repulsion between the growing structure. Fig. 15(c) illustrates the morphology of hydrates in  $\text{C}_3\text{S}$ -gypsum 5 wt%-slag A12 mixture at 3 days. Besides C–S–H gel phase and portlandite, the long needle crystal indicated the formation of ettringite in the system with gypsum. Also, a divergent fibrillary-like structure of C–S–H gel phase was observed due to the introduction of gypsum [38].

### 3.3.3. Chemical composition of C–S–H gel phase

The chemical composition of C–S–H gel phase of investigated mixtures detected by SEM-EDS point analysis is shown in Fig. 16. It should be noted that the two different types of C–S–H gel phase, i.e., inner product (IP) and outer product (OP) were not distinguished in the present paper. The Si/Ca atomic ratio of C–S–H gel phase varied from 0.4 to 1.2 in both  $\text{C}_3\text{S}$ -slag A3 and A18 mixtures without gypsum. The trend of Al/Ca atomic ratio was also similar, the majority of which was  $<0.1$ . Thus, the Ca/Si and Al/Si atomic ratios of C–S–H gel phase formed in mixtures without gypsum seemed to be independent of  $\text{Al}_2\text{O}_3$  content of slag.

For mixtures with gypsum, the Si/Ca atomic ratio of C–S–H gel phase fluctuated a little bit, still varying from 0.4 to 1.2. However, significant more Al in the matrix was observed in these two mixtures. When there was attraction from sulfate, besides that fixed in hydrotalcite-like phase, the rest  $\text{Al}^{3+}$  ions would enter into the matrix,

either take part in the formation of ettringite or be absorbed into C–S–H (A)–H gel phase, resulting in a higher Al/Si ratio. On the other hand, it was also pointed out in [39] that the degree of polymerization of C–S–H gel phase at this early age may not be sufficient for Al to be accommodated within the structure. At least, it was more likely that the aluminum existed in ettringite and/or monosulfate layers intermixed with C–S–H gel phase layers.

### 3.4. Thermodynamic modelling

To verify the results of the above measurements, thermodynamic modelling was carried out using the Gibbs free energy minimization program GEMS [40,41] with thermodynamic data from the PSI-GEMS database [42,43] supplemented by cement specific data [44,45]. The calcium-alkali aluminosilicate hydrate ideal solid solution model (CNASH<sub>ss</sub>) proposed by Myers et al. [46] was employed to describe the C–A–S–H gel phase in the system. MA-OH-LDH<sub>ss</sub> containing three end-members with Mg/Al ratios of 2, 3 and 4 reformulated into an ideal solid solution was used to perform the modelling of hydrotalcite-like solid solution series [47]. For simplicity, some assumptions were introduced. For example, reactants of different hydration degrees were assumed, and it was postulated that slag dissolved congruently. The used hydration degree was 80 % for  $\text{C}_3\text{S}$ , 100 % for gypsum, and 15 % for slag at 3 days. Moreover, the modelling did not consider the difference of hydration degree among slags, and it only reflected equilibrium phase assemblage accounting for thermodynamic approach.

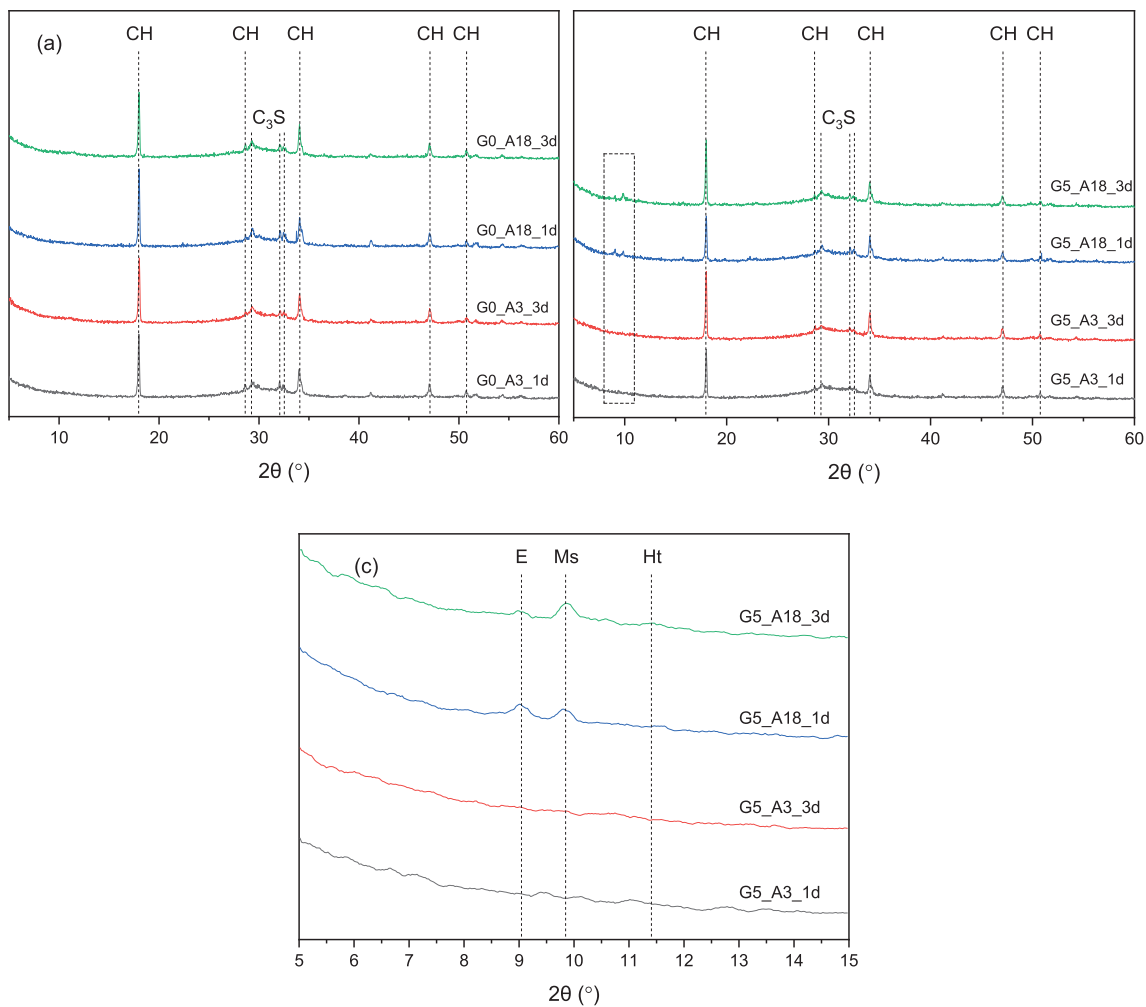


Fig. 13. Exemplary results of XRD analysis of specimens (a) without gypsum (b) with gypsum at 1 and 3 days; (c) zoom in the rectangle area from 5 to 15° ( $2\theta$ ) in (b). CH: portlandite; E: ettringite; Ms: calcium monosulfaluminate; Ht: hydrotalcite-like phase.

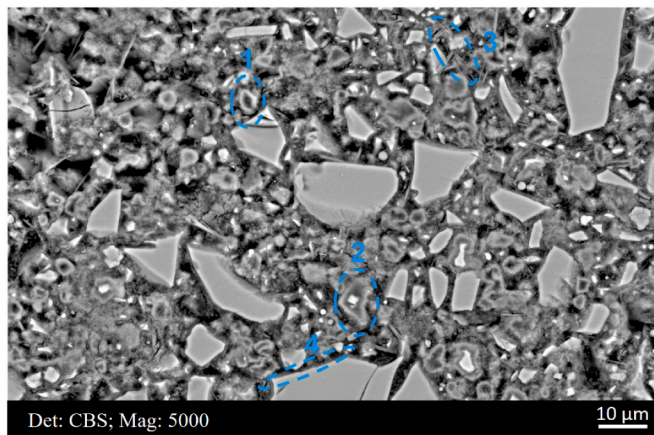


Fig. 14. Microstructure of  $C_3S$ -5 wt% gypsum-slag A18 blend after 3 days of curing. 1: Hadley grain and hollow hydration shell was formed; 2: a clear grey level difference between the outer product and inner product formed around partially hydrated  $C_3S$  grain; 3: fine and compact crystal of monosulfate; 4: hydrates formed around partially hydrated slag particle.

### 3.4.1. Effect of $Al_2O_3$ content of slag

Fig. 17 elaborates the impact of  $Al_2O_3$  content in slag on the volume of phase assemblage with 5 wt% gypsum addition. Increasing  $Al_2O_3$

content from 3.69 (slag A3) to 18.19 wt% (slag A18) firstly increased the amount of ettringite formed until the consumption of gypsum (labelled as point P1 in the graph). Then, ettringite content stabilized with the continuous increase of  $Al_2O_3$  content until the transformation from ettringite to monosulfate started (labelled as point P2 in the graph.). For slag with few  $Al_2O_3$ , it was supposed that all  $Mg^{2+}$  ion dissolved from slag was bound into magnesium silicate hydrate (M-S-H) rather than brucite ( $Mg(OH)_2$ ) owing to its low diffusion ability [48,49], and when adequate  $Al_2O_3$  content was accumulated, all magnesium entered into hydrotalcite-like phase due to its lower solubility product (Ksp) compared with M-S-H.

Gypsum was surplus when slag contained few  $Al_2O_3$  as revealed in the modelling, which was consistent with the results shown in Fig. 8(a), and it was thus concluded that for  $C_3S$ -gypsum-slag A3 blend, gypsum was sufficient to react with  $Al^{3+}$  ion dissolved from slag. As for slag A12 and A18 blends, the availability of gypsum was the rate-controlling factor. The results from modelling were also in agreement with the change of phase assemblage reflected by TGA (Fig. 12) and XRD (Fig. 13). The formation of monosulfate became increasingly prominent with additional  $Al_2O_3$  content. It was also noted that the portlandite content decreased significantly upon the occurrence of monosulfate. These results verified the following equation for the formation of monosulfate involving the participate of ettringite, portlandite, and aluminate dissolved from slag, i.e.,

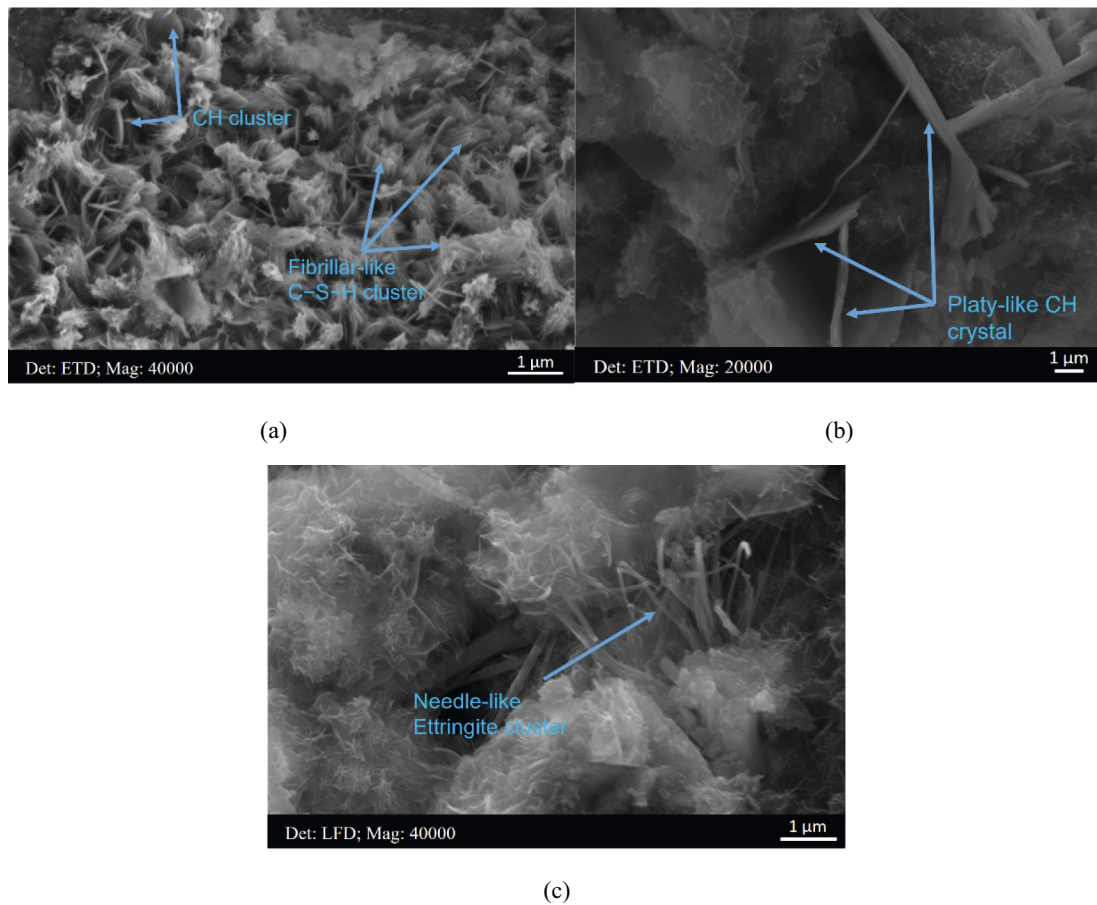
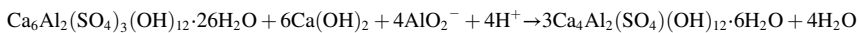


Fig. 15. Morphology of different hydrates of (a) and (b) C<sub>3</sub>S-slag A12 blend at 3 days; (c) C<sub>3</sub>S-5 wt% gypsum-slag A12 blend at 3 days. CH: portlandite.



### 3.4.2. Effect of gypsum

Fig. 18 elaborates the impact of gypsum addition on the phase assemblage based on C<sub>3</sub>S-gypsum-slag A18 blend. The volume of monosulfate increased gradually at the beginning when alumina dissolved from slag was sufficient, and it prevented the formation of ettringite; however, ettringite started to occur with the continuous addition of gypsum (labelled as point P in the graph), implying that adequate sulfate favored the precipitation of ettringite.

It was important to note that the stabilization of ettringite with the addition of extra sulfate led to a remarkable increase in the volume of hydrates. Before point P circled in the graph, the total volume changed slightly, whereas it increased apparently with the formation of ettringite although the volumes of C-S-H gel phase and monosulfate decreased. This phase contributes a lot to space filling [51].

Collectively, dependent of the alumina content of slag and gypsum content added, aluminum dissolved from slag contributed to the aluminate reaction significantly. Therefore, when calculating SO<sub>3</sub>/Al<sub>2</sub>O<sub>3</sub> ratio, alumina content of slag should also be taken into consideration. Especially for slag with high Al<sub>2</sub>O<sub>3</sub> content (slag A18 in this paper), approximately 8 wt% of gypsum was requested to maximum the amount of ettringite that can be produced at 3 days. Meanwhile, the

sulfur species in commercial slag acted a similar role as sulfate dissolved from gypsum. In the following research, the authors would extend the C<sub>3</sub>S-gypsum-slag system to C<sub>3</sub>S-C<sub>3</sub>A-gypsum-slag system, and compare it with real cement-slag system, to promote the understanding of hydration characteristics of slag-rich cement paste at early age.

## 4. Conclusions

The present research investigated the hydration characteristics of C<sub>3</sub>S-gypsum-slag system at early age. As shown above, the interaction among C<sub>3</sub>S, sulfate (gypsum) and Al<sub>2</sub>O<sub>3</sub> (slag) was complex, and conclusions were mainly obtained based on aluminate reaction:

- Al<sup>3+</sup> had a perturbing effect on the reactivity of silicate, and the more Al<sub>2</sub>O<sub>3</sub> in slag, the longer of induction period. Gypsum itself had little impact on the hydration of C<sub>3</sub>S; however, when slag and gypsum were added together into the system, the duration of dormant period was reduced.
- The onset of aluminate peak in the calorimetric curve occurred at a similar timing (~15 h after mixing) or cumulative heat release (~400 J/g C<sub>3</sub>S) for all mixtures irrespective of the amount of Al<sub>2</sub>O<sub>3</sub> in slag and gypsum content added.

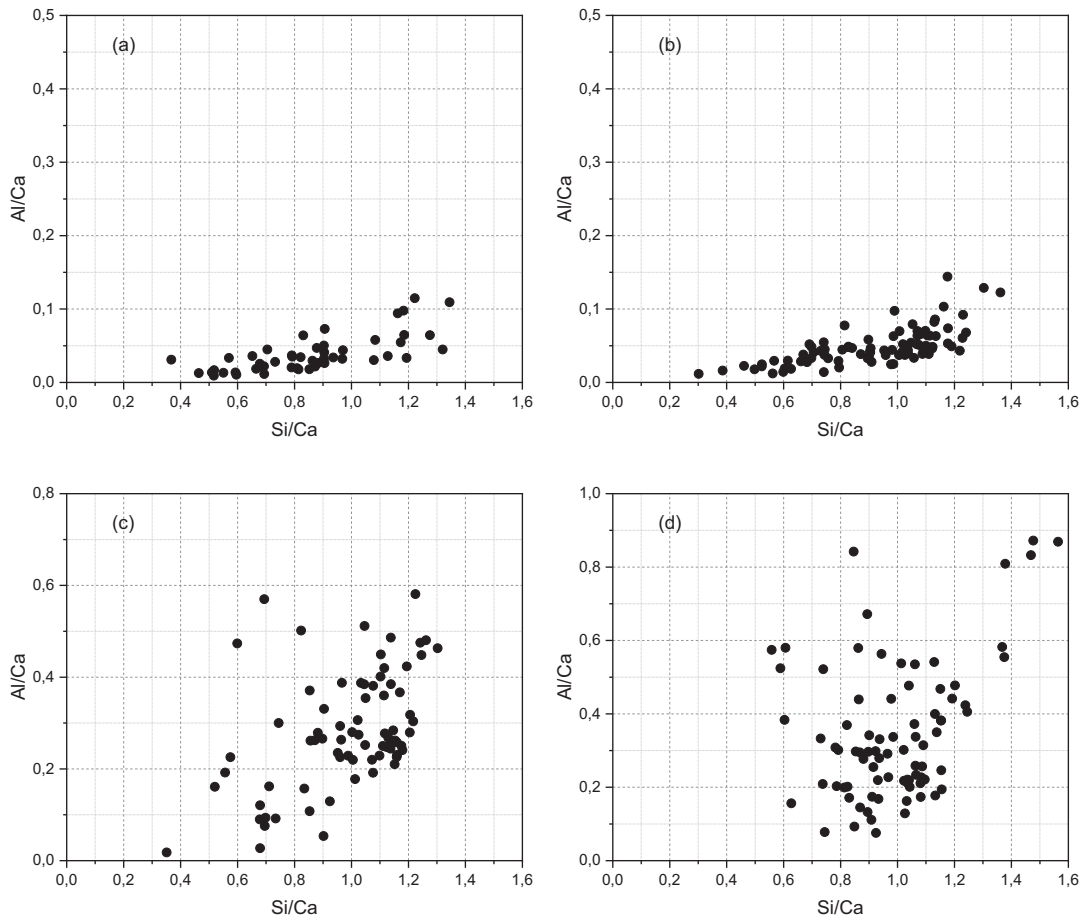


Fig. 16. Atomic ratio of Al/Ca against Si/Ca of (a) and (b) C<sub>3</sub>S-slag A3 and A18 mixtures, respectively at 3 days; (c) and (d) C<sub>3</sub>S-5 wt% gypsum-slag A3 and A18 mixtures, respectively at 3 days.

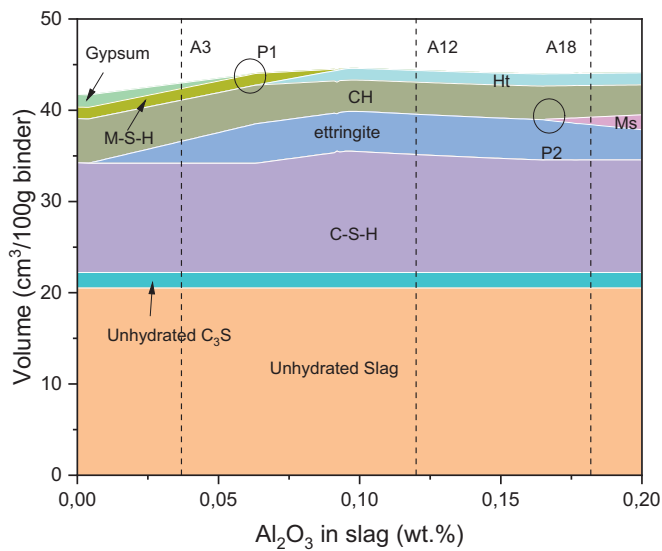


Fig. 17. Changes in the total volume of hydrates as an effect of Al<sub>2</sub>O<sub>3</sub> content of slag after 3 days of hydration. The dash lines represent three synthetic slag levels that were investigated in the present study. C<sub>3</sub>S-5 wt% gypsum-slag system was considered here. The hydration degree of C<sub>3</sub>S was calculated based on calorimetric measurement, and the hydration degree of slag was obtained based on a simple selective dissolution test [50]. Volume expressed as cm<sup>3</sup>/100 g unhydrated binder. CH: portlandite; Ht: hydrotalcite-like phase; Ms: calcium monosulfoaluminate.

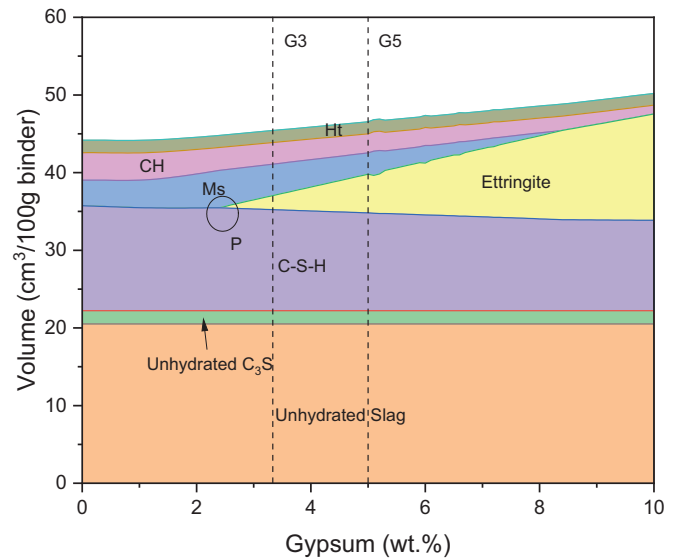


Fig. 18. Changes in the total volume of hydrates as an effect of gypsum content after 3 days of hydration. The chemical composition of slag A18 was employed in the modelling. Volume expressed as cm<sup>3</sup>/100 g unhydrated binder. CH: portlandite; Ht: hydrotalcite-like phase; Ms: calcium monosulfoaluminate.



- The rate of aluminate reaction in C<sub>3</sub>S-gypsum-slag system was controlled by the availability of SO<sub>4</sub><sup>2-</sup> and Al<sup>3+</sup> ions, thus depending on the alumina content of slag and gypsum content added significantly.
- An approximately linear correlation between SO<sub>3</sub> and Al<sub>2</sub>O<sub>3</sub> contents in the system vs. heat release from aluminate reaction was found in most mixtures investigated. Also, the heat could be taken as an indication of the amount of ettringite formed.
- Calcium monosulfoaluminate occurred in C<sub>3</sub>S-gypsum-slag A18 mixture from the first day, and its precipitation proceeded continuously with hydration at the expense of ettringite.
- Sulfur rich species incorporated in slag started to participate into the aluminate reaction after the main hydration peak of C<sub>3</sub>S, and it played a similar role to gypsum. Therefore, it was suggested to take both alumina and sulfur content in slag into consideration when calculating SO<sub>3</sub>/Al<sub>2</sub>O<sub>3</sub> ratio.

#### CRedit authorship contribution statement

Yu Zhang: Investigation, Methodology, Experiment, Analysis, Writing – Original Draft preparation, Writing – Review & Editing.

Zhi Wan: Methodology, Experiment, Analysis, Review & Editing.

Luiz Miranda de Lima Junior: Experiment, Analysis, Review & Editing.

Oğuzhan Çopuroğlu: Supervision, Funding acquisition, Review & Editing.

#### Declaration of competing interest

The authors declare no conflict of interest.

#### Data availability

Data will be made available on request.

#### Acknowledgements

The authors are grateful for the China Scholarship Council (Grant Number 201808320456, 201906220205) and BAM Infraconsult B.V. for their financial support. Authors thank Arjan Thijssen (Microlab, TU Delft) for his technical support.

#### References

- [1] L. Nicoleau, A. Nonat, D. Perrey, The di-and tricalcium silicate dissolutions, *Cem. Concr. Res.* 47 (2013) 14–30.
- [2] L. Nicoleau, A. Nonat, A new view on the kinetics of tricalcium silicate hydration, *Cem. Concr. Res.* 86 (2016) 1–11.
- [3] C. Naber, et al., Alite dissolution and CSH precipitation rates during hydration, *Cem. Concr. Res.* 115 (2019) 283–293.
- [4] A. Quennoz, K.L. Scrivener, Hydration of C3A-gypsum systems, *Cem. Concr. Res.* 42 (7) (2012) 1032–1041.
- [5] M.J. Sánchez-Herrero, A. Fernández-Jiménez, A. Palomo, Alkaline hydration of tricalcium aluminate, *J. Am. Ceram. Soc.* 95 (10) (2012) 3317–3324.
- [6] A. Quennoz, K.L. Scrivener, Interactions between alite and C3A-gypsum hydrations in model cements, *Cem. Concr. Res.* 44 (2013) 46–54.
- [7] S. Horkoss, R. Lteif, T. Rizk, Influence of the clinker SO<sub>3</sub> on the cement characteristics, *Cem. Concr. Res.* 41 (8) (2011) 913–919.
- [8] E.M.J. Berodier, EPFL, in: *Impact of the Supplementary Cementitious Materials on the Kinetics and Microstructural Development of Cement Hydration*, 2015.
- [9] E. Özbay, et al., Utilization and efficiency of ground granulated blast furnace slag on concrete properties – a review, *Constr. Build. Mater.* 105 (2016) 423–434.
- [10] N.E.A. De Belie, *Properties of Fresh and Hardened Concrete Containing Supplementary Cementitious Materials Vol. 25*, Springer, 2018.
- [11] J. Skibsted, R. Snellings, Reactivity of supplementary cementitious materials (SCMs) in cement blends, *Cem. Concr. Res.* 124 (2019), 105799.
- [12] J. Cheung, et al., Impact of admixtures on the hydration kinetics of Portland cement, *Cem. Concr. Res.* 41 (12) (2011) 1289–1309.
- [13] M. Antoni, et al., Cement substitution by a combination of metakaolin and limestone, *Cem. Concr. Res.* 42 (12) (2012) 1579–1589.
- [14] P.T. Durdziński, et al., Fly ash as an assemblage of model Ca–Mg–Na–aluminosilicate glasses, *Cem. Concr. Res.* 78 (2015) 263–272.
- [15] F.A. Zunino Sommariva, EPFL, in: *Limestone Calcined Clay Cements (LC3): Raw Material Processing, Sulfate Balance and Hydration Kinetics*, 2020.
- [16] FEHS, *Hüttensand Datei*, 2016.
- [17] Y.-F. Chai, et al., Influencing mechanism of Al<sub>2</sub>O<sub>3</sub> on sintered liquid phase of iron ore fines based on thermal and kinetic analysis, *Ironmak. Steelmak.* 46 (5) (2019) 424–430.
- [18] Y. Xue, et al., Improving high-alumina iron ores processing via the investigation of the influence of alumina concentration and type on high-temperature characteristics, *Minerals* 10 (9) (2020) 802.
- [19] F. Zunino, K. Scrivener, Factors influencing the sulfate balance in pure phase C3S/C3A systems, *Cem. Concr. Res.* 133 (2020).
- [20] W.E. Kleinjan, et al., Kinetics of the chemical oxidation of polysulfide anions in aqueous solution, *Water Res.* 39 (17) (2005) 4093–4100.
- [21] A. Gruskovnjak, et al., Hydration of alkali-activated slag: comparison with ordinary Portland cement, *Adv. Cem. Res.* 18 (3) (2006) 119–128.
- [22] B. Lothenbach, et al., Hydration of a low-alkali CEM III/B–SiO<sub>2</sub> cement (LAC), *Cem. Concr. Res.* 42 (2) (2012) 410–423.
- [23] B. Bickmore, The effect of adsorbed Al(OH)<sub>4</sub><sup>-</sup> on the dissolution rate of quartz, in: *Eleventh Annual VM Goldschmidt Conference*, 2001.
- [24] X. Pardal, et al., <sup>27</sup>Al and <sup>29</sup>Si solid-state NMR characterization of calcium-aluminosilicate-hydrate, *Inorg. Chem. Front.* 51 (3) (2012) 1827–1836.
- [25] T. Chappex, K.L. Scrivener, The effect of aluminum in solution on the dissolution of amorphous silica and its relation to cementitious systems, *J. Am. Ceram. Soc.* 96 (2) (2013) 592–597.
- [26] L. Nicoleau, E. Schreiner, A. Nonat, Ion-specific effects influencing the dissolution of tricalcium silicate, *Cem. Concr. Res.* 59 (2014) 118–138.
- [27] P. Suraneni, R.J. Flatt, Use of micro-reactors to obtain new insights into the factors influencing tricalcium silicate dissolution, *Cem. Concr. Res.* 78 (2015) 208–215.
- [28] F. Begarin, et al., Hydration of alite containing aluminium, *Adv. Appl. Ceram.* 110 (3) (2011) 127–130.
- [29] E. Pustovgar, et al., Influence of aluminates on the hydration kinetics of tricalcium silicate, *Cem. Concr. Res.* 100 (2017) 245–262.
- [30] V. Kocaba, *Development and Evaluation of Methods to Follow Microstructural Development of Cementitious Systems Including Slags*, EPFL, 2009.
- [31] S. Bergold, F. Goetz-Neunhoeffer, J. Neubauer, Interaction of silicate and aluminate reaction in a synthetic cement system: implications for the process of alite hydration, *Cem. Concr. Res.* 93 (2017) 32–44.
- [32] I. Odler, J. Colán-Subauste, Investigations on cement expansion associated with ettringite formation, *Cem. Concr. Res.* 29 (5) (1999) 731–735.
- [33] P. Chaunsali, P. Mondal, Hydration and early-age expansion of calcium sulfoaluminate cement-based binders: experiments and thermodynamic modeling, *J. Sustain. Cement Based Mater.* 5 (4) (2016) 259–267.
- [34] F.P. Glasser, et al., Modification of cement pore fluid compositions by pozzolanic additives, *Cem. Concr. Res.* 18 (2) (1988) 165–178.
- [35] A. Roy, Sulfur speciation in granulated blast furnace slag: an X-ray absorption spectroscopic investigation, *Cem. Concr. Res.* 39 (8) (2009) 659–663.
- [36] K.Y. Chen, J.C. Morris, Kinetics of oxidation of aqueous sulfide by oxygen, *Environ. Sci. Technol.* 6 (6) (1972) 529–537.
- [37] J. Couvidat, et al., Greening effect of concrete containing granulated blast-furnace slag composite cement: is there an environmental impact? *Cem. Concr. Compos.* 113 (2020), 103711.
- [38] B. Mota, T. Matschei, K. Scrivener, The influence of sodium salts and gypsum on alite hydration, *Cem. Concr. Res.* 75 (2015) 53–65.
- [39] H.F. Taylor, *Cement Chemistry Vol. 2*, Thomas Telford London, 1997.
- [40] T. Wagner, et al., GEM-selektor geochemical modeling package: TSolMod library and data interface for multicomponent phase models, *Can. Mineral.* 50 (5) (2012) 1173–1195.
- [41] D.A. Kulik, et al., GEM-selektor geochemical modeling package: revised algorithm and GEMS3K numerical kernel for coupled simulation codes, *Comput. Geosci.* 17 (1) (2013) 1–24.
- [42] W. Hummel, *Nagra Technical Report NTB 02-16*, Wettingen, Switzerland, 2002.
- [43] W. Hummel, et al., *Nagra/PSI chemical thermodynamic data base 01/01*, *Radiochim. Acta* 90 (9–11) (2002) 805–813.
- [44] T. Matschei, et al., Thermodynamic properties of Portland cement hydrates in the system CaO–Al<sub>2</sub>O<sub>3</sub>–SiO<sub>2</sub>–CaSO<sub>4</sub>–CaCO<sub>3</sub>–H<sub>2</sub>O, *Cem. Concr. Res.* 37 (10) (2007) 1379–1410.
- [45] B. Lothenbach, et al., Thermodynamic modelling of the effect of temperature on the hydration and porosity of Portland cement, *Cem. Concr. Res.* 38 (1) (2008) 1–18.
- [46] R.J. Myers, S.A. Bernal, J.L. Provis, A thermodynamic model for C-(N)-ASH gel: CNASH.ss. Derivation and validation, *Cem. Concr. Res.* 66 (2014) 27–47.
- [47] R.J. Myers, et al., Thermodynamic modelling of alkali-activated slag cements, *Appl. Geochem.* 61 (2015) 233–247.
- [48] L. Mo, D.K. Panesar, Effects of accelerated carbonation on the microstructure of Portland cement pastes containing reactive MgO, *Cem. Concr. Res.* 42 (6) (2012) 769–777.
- [49] M. Sajid, et al., Understanding the structure and structural effects on the properties of blast furnace slag (BFS), *ISIJ Int.* 59 (7) (2019) 1153–1166.
- [50] V. Kocaba, E. Gallucci, K.L. Scrivener, Methods for determination of degree of reaction of slag in blended cement pastes, *Cem. Concr. Res.* 42 (3) (2012) 511–525.
- [51] P. Termkhajornkit, et al., Dependence of compressive strength on phase assemblage in cement pastes: beyond gel–space ratio—experimental evidence and micromechanical modeling, *Cem. Concr. Res.* 56 (2014) 1–11.